scientific reports

Check for updates

OPEN

Development of a Disease Modeling Framework for Glutamatergic Neurons Derived from Neuroblastoma Cells in 3D Microarrays

Duc Long Nguyen[1,4], My Phuong Thi Le[1,4], Kyung Won Lee[1,2], Jae-Ho Kim[1,3], Hyun C. Yoon[1,2]✉ & Huyen T. M. Pham[1]✉

Neurodegenerative diseases (NDDs) present significant challenges due to limited treatment options, ethical concerns surrounding traditional animal models, and the time-consuming and costly process of using human-induced pluripotent stem cells (iPSCs). We addressed these issues by developing a 3D culture protocol for differentiating SH-SY5Y cells into glutamatergic neurons, enhancing physiological relevance with a 3D microarray culture plate. Our protocol optimized serum concentration and incorporated retinoic acid (RA) to improve differentiation. We analyzed the proportions of N-type and S-type cells, observing that RA in the maturation stage not only reduced cell proliferation but also enhanced the expression of MAP2 and VGLUT1, indicating effective neuronal differentiation. Our approach demonstrates the strong expression of glutamatergic neuron phenotypes in 3D SH-SY5Y neural spheroids, offering a promising tool for high-throughput NDD modeling and advancing drug discovery and therapeutic development. This method overcomes limitations associated with conventional 2D cultures and animal models, providing a more effective platform for NDD research.

Keywords SH-SY5Y cells, 3D microarrays, Glutamatergic neuron, Disease modeling, Retinoic acid

Neurodegenerative diseases (NDDs) caused by uncontrolled neuronal death and the loss of structure and function of neural networks have detrimentally influenced the lives of more than 50 million people worldwide[1]. Dementia, which is a syndrome associated with various NDDs such as Alzheimer's disease, Tauopathies, Huntington's disease, and Parkinson's disease, is expected to cost the world $2.8 trillion in 2030, including direct medical, indirect medical, and informal care costs[1]. The complex pathogenesis and unmanageable environmental and genetic factors hinder the efficacy of treatment attempts. Rodents have long served as models for studying NDDs. However, alongside ethical concerns of animal models, this method is costly, time-consuming, and unable to fully mimic human diseases[2]. Thus, the development of a human-based in vitro model with close physiological resemblance may shed new light on NDD modeling and drug discovery. Human induced pluripotent stem cells-derived neurons (iPSC-derived neurons) are the most prominent tools for disease modeling due to their specificity. However, generating a research-grade iPSC line can take 3–4 weeks and has an efficiency of only 0.01–0.1%[3]. Therefore, until further innovations reduce cost, time and, increase efficiencies of iPSC reprogramming, an alternative in vitro disease modeling approach is still necessary.

The SH-SY5Y cell line, originating from the bone marrow of a 4-year-old female with metastatic neuroblastoma, has been widely applied in NDD research[4,5]. These cells, derived from a human source, express many human-specific proteins and isoforms not present in rodent models[6]. As an immortalized cell line, SH-SY5Y cells can proliferate indefinitely, allowing for large-scale production and serving as a cost-effective model. The cell line has been reported to differentiate into neurons and express neuronal markers such as Synapsin 1 (SYN1), microtubule-associated protein 2 (MAP2), or tubulin beta class III (TUJ1) and facilitate several types of neurotransmitter communications[7–9]. Easier to handle than animal models and primary neurons SH-SY5Y can

[1]Department of Molecular Science and Technology, Ajou University, Suwon 16499, South Korea. [2]Advanced College of Bio-convergence Engineering, Ajou University, Suwon 16499, South Korea. [3]ANK corporation, TheANK, Suwon 16522, South Korea. [4]Duc Long Nguyen and My Phuong Thi Le contributed equally to this work. ✉email: hcyoon@ajou.ac.kr; minhhuyen.ks.nb@gmail.com

be genetically modified to introduce disease-related mutations or gene expression constructs[10–12]. Furthermore, as a cell line, SH-SY5Y bypasses the ethical issues associated with animal models.

While the 2D culture of SH-SY5Y cells has been instrumental in elucidating various aspects of neuronal biology and disease mechanisms[5,8,11,13–18], it has several limitations. These include the inability to mimic the complex 3D microenvironment of the brain, limited cell-cell and cell-matrix interactions, and altered cell morphology and behavior compared to in vivo conditions[19]. Due to their lack of complexity, traditional 2D cultures may not fully recapitulate certain aspects of neuronal physiology and pathology[20]. However, research on differentiation using 3D methods is limited because these processes are time-consuming, labor-intensive, difficult to control, and challenging to mass-produce and apply for downstream applications.

While differentiation and maturation protocols towards dopaminergic, cholinergic, and adrenergic neurons are established[5,18,19], the approach for glutamatergic and GABA neurons is very limited[7]. Additionally, most studies focus on qualitative analysis, reporting the existence of targeted neurons without quantifying the amount of neuroplastic (N-type) and sub-adherent(S-type) cells or proportions of neuron types after differentiation and maturation. S-type cells are epithelial-like cells with characteristics of Schwann cells. Due to their non-neuronal and high proliferative features, S-type cells are unwanted products of SH-SY5Y differentiation. At the same time, N-type cells are neuronal-like ones that adopt neuronal phenotypes and are suitable for neural-related studies[13].

PAMCELL™ plates were 3D microarray plates designed to produce large quantities of uniformly sized spheroids. Each well of the plate contains 350 100-µm round micropads formed by monolayer of 700 nm arginine-glycine-aspartate (RGD) peptide-coated silica particles. Due to strong binding affinity of integrin on the cell membrane and RGD peptide on the surface of micropad, the cell can migrate from non-adhesive polyethylene glycol (PEG) surface to designated areas and form size-defined spheroids. Unlike other spheroid culture plates, the bottom layer of the plates is made from Cyclo Olefin Polymer (COP) thin film, allowing users to directly perform downstream applications such as immunofluorescence and scanning electron microscopy (SEM) on the plate[21,22].

Thus, to overcome the limitations of traditional 2D cultures and the challenges associated with 3D differentiation methods, our research focuses on developing a large-scale 3D culture protocol for differentiating and maturing SH-SY5Y cells into neurons with glutamatergic phenotype using the 96-well R100 PAMCELL™ microarray plate. By optimizing serum concentration and incorporating retinoic acid (RA) in the 3D culture environment, we aim to enhance the differentiation process and create a more physiologically relevant model for studying NDDs. This approach not only facilitates high-throughput NDD modeling but also paves the way for more effective drug discovery and therapeutic development.

Results

Morphological analysis of differentiated SH-SY5Y cells in 2D and 3D culture systems

To address the impact of RA in maturation stage (stage II), 2D and 3D SH-SY5Y cells were cultured and differentiated in 4 different kinds of media: growth media (EMEM, 15% hiFBS, 1% PS), differentiation media (EMEM, 2.5% hiFBS, 10 µM RA, 1% PS) and 2 variants of maturation media (Neurobasal, 1% B27, 20 mM KCl, 2 mM Glutamax, 0.05 ng/µL BDNF, 1% PS): RA free and RA treated (10 µM). Additionally, in the differentiation stage (stage I) 3D culture cells were examined with 2 different serum concentrations (2.5% and 5%) due to the difference in metabolic demands. Cellular morphology was observed every day under an inverted microscope.

On the final day of Stage I, 2D SH-SY5Y cells exhibited significant morphological changes indicative of differentiation into N-type cells, characterized by the outgrowth of neurites (Fig. 1A). Despite this differentiation, some S-type and undifferentiated cells were still observed. After 6-day stage II, in media containing RA, the cells adopted a triangular shape and developed dense neurite networks. Although some undifferentiated cells persisted, the majority had acquired a neuron-like phenotype. Conversely, in RA-free media, there was an increase in the population of undifferentiated cells and S-type SH-SY5Y cells, which retained their flat, large, and polygonal shape.

Before being treated with differentiation media, the cells in 3D PAMCELL™ plates were nurtured in growth media for 2–3 days to form spheroids (Fig. 1B). After the 12-day differentiation process, the size of the spheroids was measured. Spheroids differentiated in 2.5% hiFBS had an average diameter of 111.92 ± 33.19 µm ($n = 50$) in the presence of RA in maturation media and 110.11 ± 31.88 µm in RA-free media, whereas those in 5% hiFBS were larger and exhibited less size variation, with an average diameter of 125.72 ± 19.50 µm in RA-treated media and 131.38 ± 27.08 µm in RA-free media (Fig. 1C). This demonstrates the impact of serum on spheroid proliferation. Additionally, while RA affected the morphology of 2D cells, it did not significantly impact spheroid size.

Flow cytometry analysis of serum concentration and the effect of RA in maturation media

The observation of cellular morphology was a confirmation of the presence of mature-like SH-SY5Y neurons. Subsequently, we further quantified the amount of differentiation cells via flow cytometry analysis (FACS). The expression of neurogenic markers MAP2, vesicular glutamate transporter 1 (VGLUT1), and Tyrosine Hydroxylase (TH) in SH-SY5Y cells were measured under different conditions. 2D cells were cultured with 2.5% hiFBS, and 3D samples were nurtured with 2.5% hiFBS and 5% hiFBS. The analysis was conducted on day 6, following the completion of the differentiation stage, and on day 12, after the maturation stage had concluded.

Figure 2A illustrates the FACS analysis from day 6. While over 70% of events obtained from 2D cultures with 2.5% hiFBS and 3D cultures with 5% hiFBS were cells, only 30% of events in 3D spheroids differentiated in 2.5% hiFBS were considered similar, and these cells did not express any neurogenic markers. By day 12, 3D cultures in 2.5% hiFBS showed a healthier profile, with over 80% of the total 30,000 events being cells, 69.27% of which expressed the MAP2 signal and 90.06% expressed VGLUT1 (Fig. 2B). This suggests that 2.5% hiFBS requires

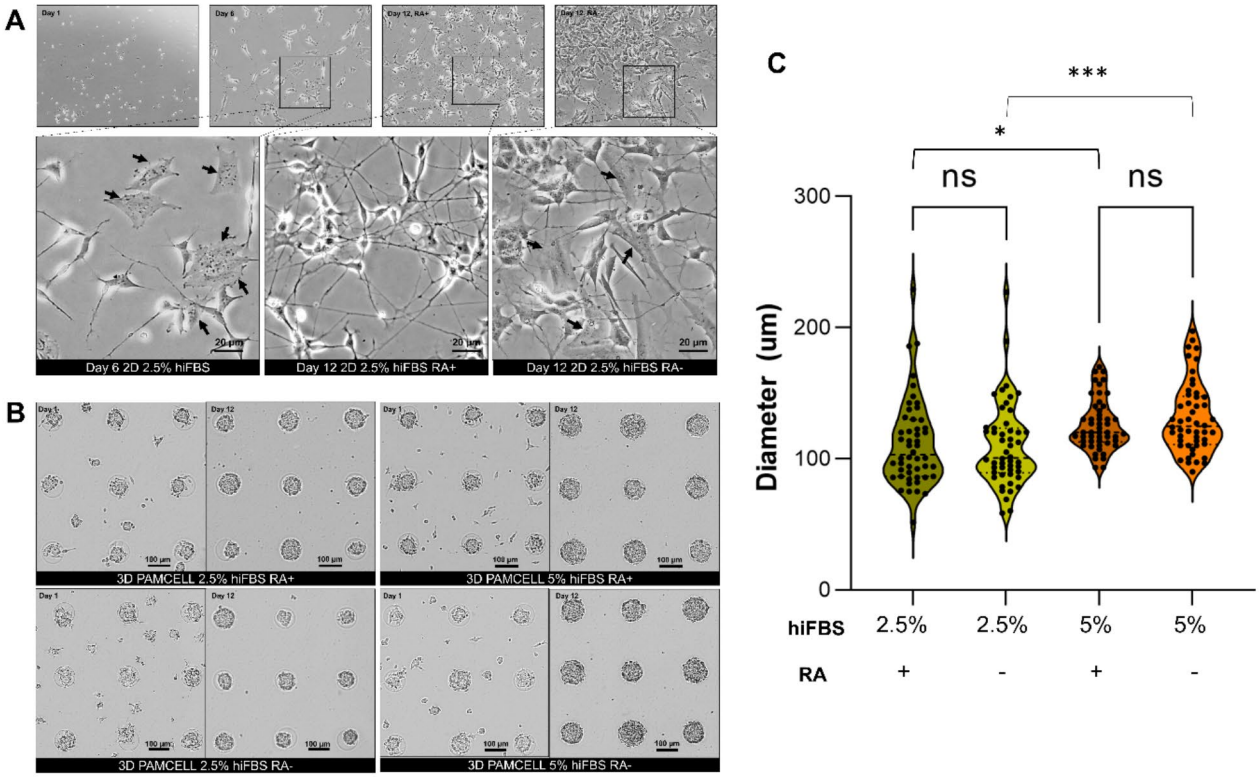

Fig. 1. Morphology of differentiated SH-SY5Y cells in 2D and 3D PAMCELL cultures with/without RA in maturation media and different serum conditions. **(A)** Bright-field images of SH-SY5Y in 2D culture on day 1, day 6, and day 12. The arrow (black) indicates the S-type cells, which is flat and stretch on surface. Images were captured using an inverted epifluorescence microscope at 60X magnification in phase contrast. **(B)** Bright-field images of SH-SY5Y spheroids on day 1 and day 12. **(C)** Violin plots of the size of spheroids cultured in different serum concentrations. Diameters of 50 random spheroids were measured. Significant differences between different cultured conditions were evaluated. (ns = not significant, $^{*}p < 0.05$, $^{***}p < 0.001$, unpaired Student's t-test).

additional time for differentiation and maturation, and the serum concentration may not be sufficient for the spheroids to maintain both their metabolic status and differentiation.

Conversely, the analysis of 2D cultures in 2.5% hiFBS and 3D cultures in 5% hiFBS on day 6 showed that over 84% of single cells were positive for the MAP2 signal, indicating successful differentiation (Fig. 2A). Interestingly, while the TH signal was expressed in only 10.77% of 2D cultures in 2.5% hiFBS and 12.09% in 3D cultures in 5% hiFBS, 93.8% of 2D cells and 81.14% of 3D cells expressed the VGLUT1 signal, suggesting that the cells were differentiating towards a glutamatergic pathway.

Figure 2B highlights the importance of RA in the maturation media when 38.67% of the 2D cell population in 2.5% hiFBS cultured in RA-free media were negative for the MAP2 signal. The results suggest that the cells continued proliferating in RA-free media, leading to the emergence of unwanted undifferentiated cells. The 3D cultures in 5% hiFBS negated the impact of the absence of RA, maintaining 88.81% of cells expressing the MAP2 signal. However, their mean signal intensity reduced from 312,048 to 159,333.

To verify the effect of RA, we compared the FACS results of 2D cells and 3D cells cultured with 5% hiFBS after a 12-day maturation period, with and without RA (Fig. 2C, D). On 2D cultures, the proportion of MAP2-positive cells increased from 61.33 to 93.25% when RA was added to the maturation media. VGLUT1 also expressed the same result from 79.43% cells population to 93.25%. In 3D cells cultured in 5% hiFBS, the presence of RA also led to enhanced signals, with the mean MAP2 and VGLUT1 signals increasing fourfold and sixfold, respectively. These results suggest that RA not only inhibited unwanted proliferation but also promoted the maturation of SH-SY5Y cells in both 2D and 3D culture conditions. The contrast in signals between TH and VGLUT1 further supports the differentiation of neurons towards a glutamatergic pathway.

Additionally, the 3D PAMCELL™ culture with 5% hiFBS demonstrated superior expression of the neurogenic markers MAP2 and VGLUT1 on both day 6 and day 12. This suggests that the 3D PAMCELL™ in 5% hiFBS condition is more optimal for the differentiation and maturation of SH-SY5Y cells. Therefore, we recommend using 3D 5% hiFBS for further studies on SH-SY5Y cell differentiation and maturation.

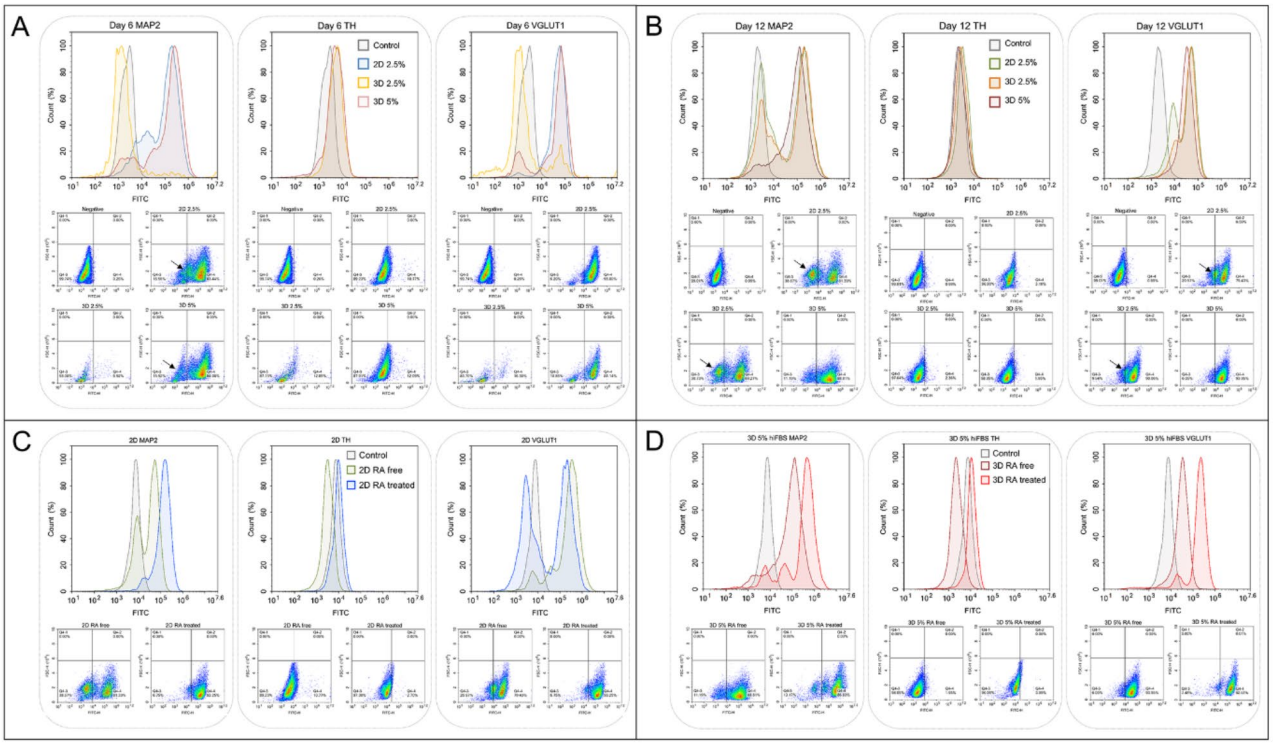

Fig. 2. Differentiation and maturation of SH-SY5Y cells in 2D and 3D cultures assessed by flow cytometry analysis. **(A)** FACS analysis on day 6 of differentiation. The black arrow indicated the population of undifferentiated cells **(B)** FACS analysis of cells cultured in maturation media without RA. The black arrow indicates the population of undifferentiated **(C)** Comparison of neuronal marker expression in 2D cell cultures with and without RA treatment. **(D)** Comparison of neuronal marker expression in 3D spheroids cultured in 5% hiFBS with and without RA treatment.

Immunocytochemical and mRNA expression analysis of neuronal differentiation and maturation

Five mature neuronal markers were analyzed by immunocytochemistry (ICC), as shown in Fig. 3. Figure 3A illustrates the expression of VGLUT1, a key indicator for glutamatergic neurons[23]. VGLUT1 was strongly expressed across all conditions, confirming the differentiation protocol's effectiveness towards a glutamatergic pathway. Served as vesicular glutamate transporters that transported glutamate into synaptic vessels in neurotransmission, VGLUT1 is localized in axon ends and is an important marker for presynaptic terminal development. Additionally, glutamate is an impactful regulator on generation of contact dendrites[23–25]. Thus, in the 3D 5% hiFBS condition, VGLUT1 was prominently expressed on the outer layer of the spheroid, suggesting a distinct orientation of the neurons and their connections.

MAP2, essential for dendritic elongation and structural integrity of neurons[26], was observed differently across conditions. In the 3D 2.5% hiFBS spheroids, MAP2 was expressed as short but thick lines, indicating the early stage of neurite extension (Fig. 3C). Conversely, in the 3D 5% hiFBS spheroids, MAP2 appeared as thin, long, and branching lines around the spheroid. Additionally, different media conditions directly affected the ability to outgrow the neurites of spheroids. While neurites in 5% hiFBS-growth spheroids had average 53.43 ± 17.39 µm in length, spheroid treated in 2.5 hiFBS only extended neurites with 30.66 ± 10.93 µm in length. These suggest that spheroids in 5% hiFBS are at a more mature stage of neuronal development than lower serum concentration one. (Supplementary Table S6 and Figure S2).

The expression of TUJ1 reinforced similar observations (Fig. 3D). 3D 2.5% hiFBS spheroid only expressed TUJ1 in outer layer cells while 3D 5% hiFBS spheroid displayed a more complex axonal matrix at the center, indicating a higher degree of maturation.

Synapsin plays a key role in the regulation of neurotransmitter release and serves as a reliable marker for presynaptic vesicles[27]. Similarly, EN1 (Engrailed-1) is crucial for interneuron communication and has been shown to play an important role in neuronal survival. The deletion of EN1 results in the death of neurons in the ventral nuclei of the lateral lemniscus during development[28]. These roles of Synapsin and EN1 suggest that their expression across the spheroids indicate synaptic activities inside the spheroid. (Fig. 3B, E).

Additionally, Fig. 3F highlights the height of spheroids as visualized through depth-coded imaging with TUJ1 staining, showing that the representative spheroid had an approximate height of 70 µm along the z-axis and a diameter of around 100 µm in the x and y axes. The spheroid formation image also illustrates the uniformity of spheroids, further supporting the consistency of the model used.

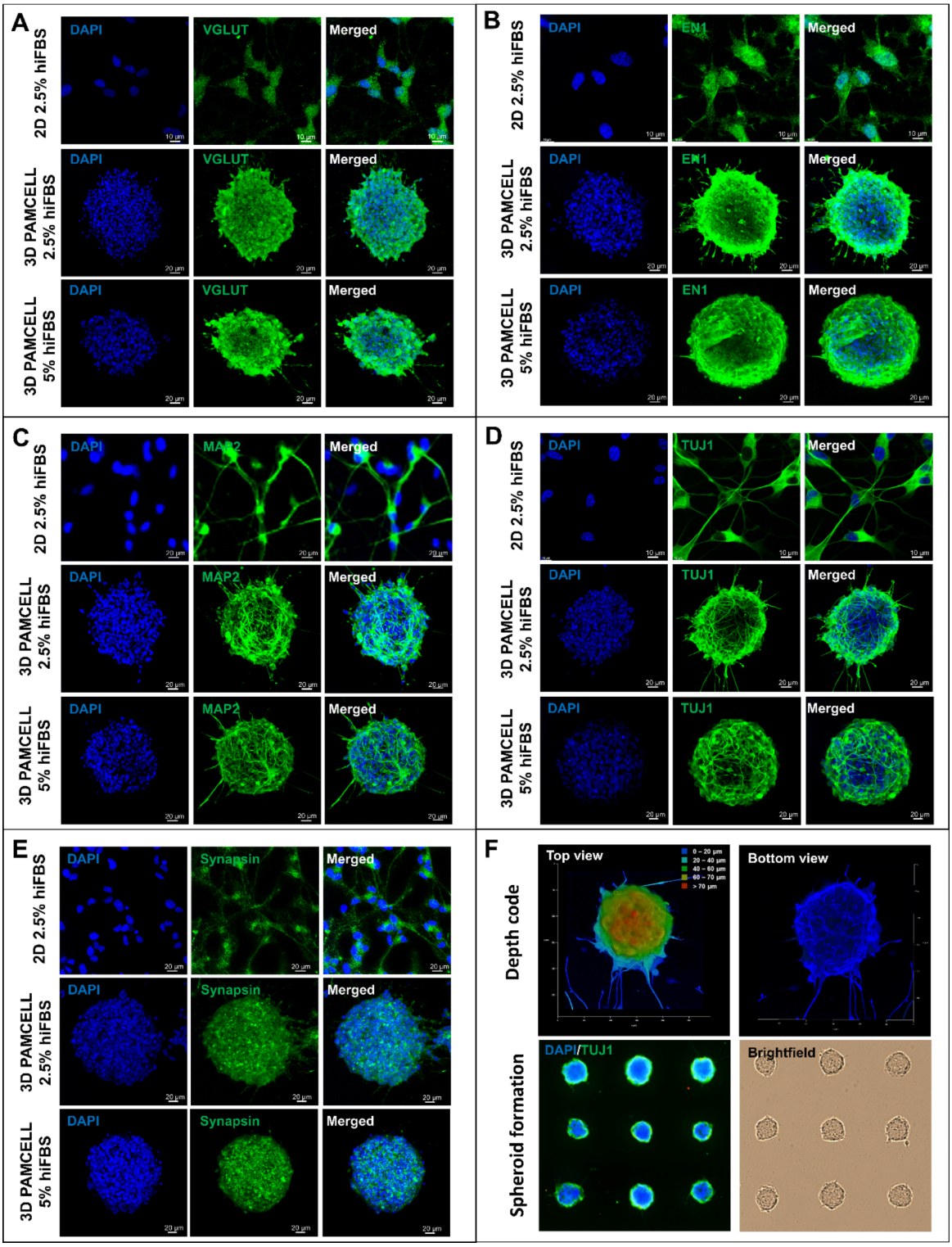

Fig. 3. Expression of mature neuronal markers by 2D, 3D 2.5% hiFBS and 3D 5% hiFBS after 12-day maturation in presence of RA. **(A)** Expression of VGLUT1. **(B)** Expression of EN1. **(C)** Expression of MAP2. **(D)** Expression of TUJ1. **(E)** Expression of Synapsin. **(F)** Depth code view of 3D spheroid and spheroid formation confirmation. 3D 5% hiFBS were chosen for depth code image.

The mRNA Expression Analysis (Fig. 4A) further supports that culturing cells in 3D PAMCELL™ with 5% hiFBS creates an optimal environment for SH-SY5Y differentiation and maturation.

Figure 4B, C, and D explore the impact of RA on mRNA expression levels in all 3-culture platforms and conditions. The expression levels of *MAP2*, *ENO2*, *SYN1*, and *TUBB3* were diverse among platforms. In 2D

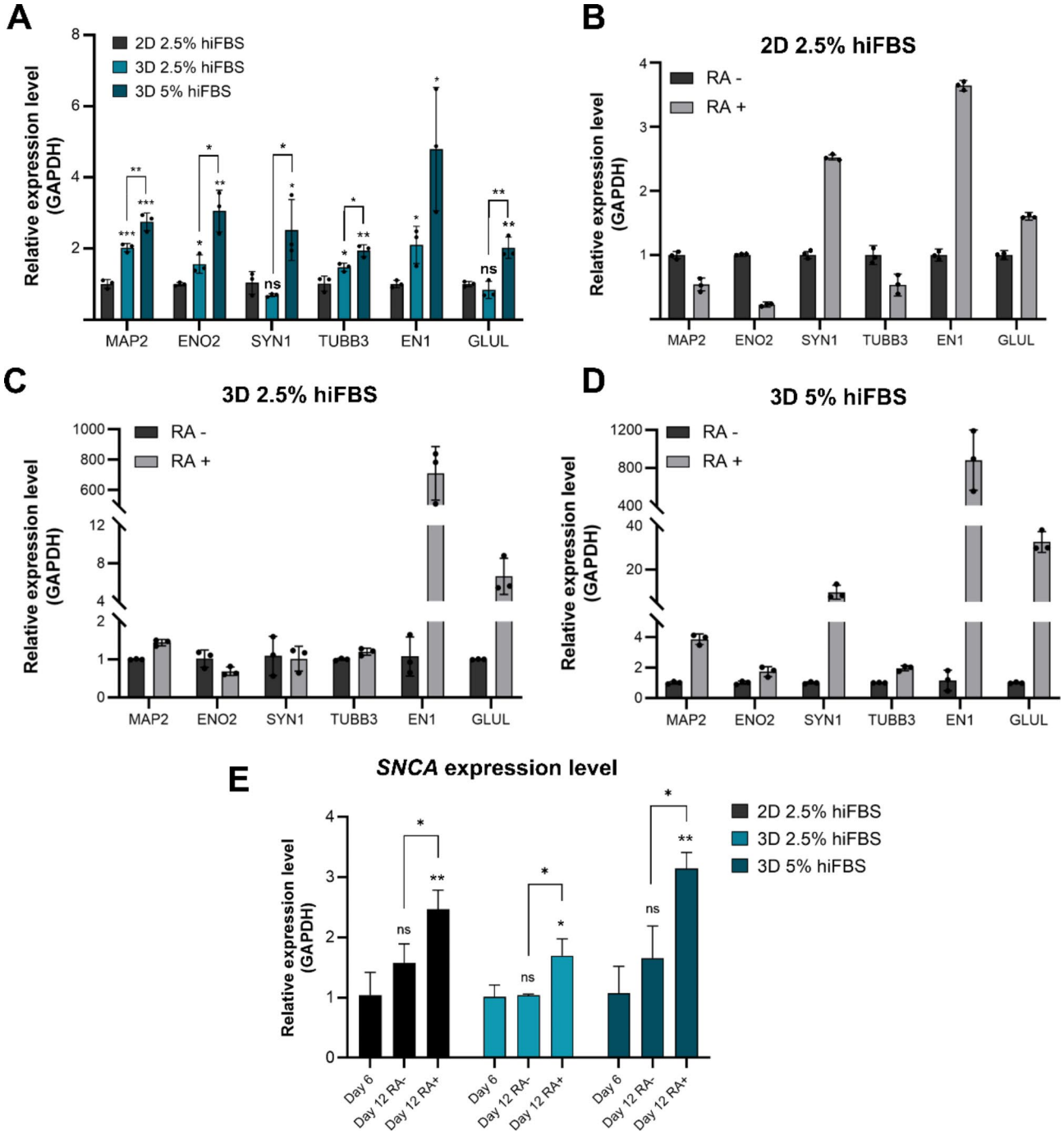

Fig. 4. Relative expression of different mature neuronal markers in 2D, 3D 2.5% hiFBS and, 3D 5% hiFBS after 12-day maturation process with and without RA. **(A)** Relative expression of 3 culture platforms and conditions with presence of RA in maturation media. Significant differences between different cultured conditions were evaluated. (ns = not significant, $*p < 0.05$, $**p < 0.01$, $***p < 0.001$, unpaired Student's t-test, $n = 3$) **(B)** The effect of RA on level of neuronal markers in 2D culture. **(C)** The effect of RA on expression level of neuronal markers in 3D 2.5% hiFBS. **(D)** The effect of RA on expression level of neuronal markers in 3D 5% hiFBS. **(E)** Serum concentration and RA effect on SNCA expression level. The vertical axis shows the relative gene expression levels as the means ± SE ($n = 03$). Bars represent the means of three replicates ± SD.

cultures with RA, there was a decrease in *ENO2* levels and no significant change in *MAP2* and *TUBB3* levels. Conversely, in 3D 5% hiFBS cultures, the levels of these markers increased, with *SYN1* and *MAP2* showing significant upregulation (9.47-fold and 3.87-fold, respectively). *EN1* and *GLUL* displayed consistent trends across all conditions, with EN1 increasing to 3.64-fold in 2D and significantly more in 3D conditions (over 710-fold in 3D 2.5% hiFBS, and over 880-fold in 3D 5% hiFBS). *GLUL* levels were 1.6 times higher in RA-treated 2D

cultures compared to RA-free conditions. In 3D cultures, RA-treated spheroids showed 6.6-fold and 32.59-fold increases in *GLUL* expression in 2.5% hiFBS and 5% hiFBS, respectively. The result suggests that RA plays a crucial role in the maturation stage of SH-SY5Y cells and significantly influences the expression levels of *EN1* and *GLUL* in the 3D culture platform. Additionally, the overexpression level of *GLUL* and VGLUT1 (Fig. 3A) indicates that the cells were expressed glutamatergic phenotype and were ready for further application.

The mRNA levels of *SNCA* were further evaluated to elucidate the effects of retinoic acid (RA) and serum concentrations on neuronal differentiation and maturation in SH-SY5Y cells (Fig. 4E). In the absence of RA treatment during stage II, *SNCA* levels on day 12 across all three conditions did not show significant improvements compared to day 6. However, upon RA treatment, SNCA levels in 2D cultures on day 12 were found to be 2.4 times higher than those measured on day 6 and 1.5 times higher than in cells nurtured without RA. For 3D cultures in 2.5% hiFBS, *SNCA* levels on day 12 with RA treatment were approximately 1.5 times higher than those on day 6 and day 12 without treatment. Notably, in 3D cells cultured in 5% hiFBS, RA treatment led to a substantial increase in *SNCA* levels, with values recorded at 2.9 times higher than on day 6 and 1.5 times higher than on day 12 without treatment.

Glutamate detection in mature-like neural spheroid using cyclic voltammetry

After confirming the protocol for mature-like neurons with glutamatergic phenotype, we proceeded to measure the levels of glutamate released as a neurotransmitter. Figure 5A illustrates the design of the electrochemical Glutamate Oxidase (GO)-modified glutamate sensor. The enzyme immobilized on the surface of a platinum (Pt) electrode catalyzes the conversion of glutamate released from the spheroid into α-ketoglutarate, producing hydrogen peroxide (H_2O_2) as a byproduct. The H_2O_2 then undergoes electrochemical oxidation at the electrode, each molecule donating two electrons. This electron flow generates an electrical current that is proportional to the glutamate concentration in the sample, allowing for quantitative analysis.

Figure 5B showed cyclic voltammograms of PBS, maturation media, healthy neural spheroids, 2-day starving spheroids, and 4-day starving spheroids. The voltammogram of the healthy neural spheroids shows a peak at 1091 µA and is higher than the peak of maturation media (633 µA). The increasing electrochemical activity is likely caused by the glutamate communication of spheroids. The current continued increase in 2-day starving spheroids and 4-day starving spheroids suggests the loss in glutamate homeostasis in spheroid led to glutamatergic hyperactivity[29]. Figure 5C further illustrates the differences in current among three types of spheroids across three independent experiments. The average peak current for healthy spheroids was 1136 ± 69 µA, while the starving spheroids showed increased average peaks of 1277 ± 71 µA for 2-day starvation and 1594 ± 152 µA for

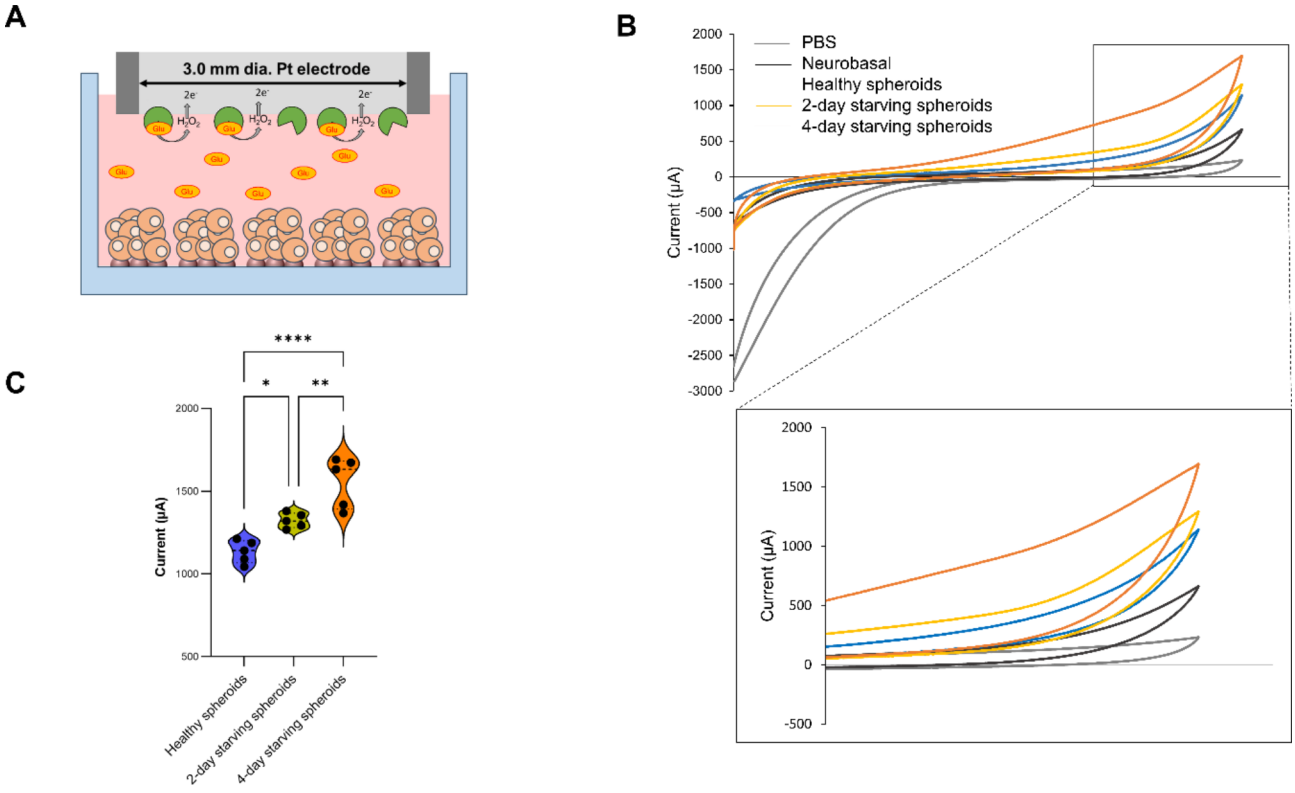

Fig. 5. Concept and result of cyclic voltammetry of enzymatic glutamate sensor. **(A)** Scheme of GO enzymatic sensor. **(B)** Detection of glutamate in 3D 5% hiFBS in different conditions. **(C)** Violin plot of current density of spheroid in different conditions (ns = not significant, $^{*}p < 0.05$, $^{**}p < 0.01$, $^{****}p < 0.0001$, unpaired Student's t-test, $n = 5$).

4-day starvation. These results suggest that the system has significant potential for application in NDD modeling and drug discovery.

Discussion

In this study, we explored the differentiation and maturation of SH-SY5Y cells into glutamatergic neurons within 3D PAMCELL™ microarrays, with a focus on optimizing serum concentrations and incorporating RA. The results provide valuable insights into the critical role of RA in the maturation process and the benefits of using 3D cultures for NDD modeling.

The differentiation and maturation of SH-SY5Y cells involve a two-stage strategy. In Stage I, RA treatment induces the expression of the tropomyosin-related kinase B (TrkB) receptor[18]. When BDNF is introduced in Stage II, the binding of BDNF to the TrkB receptor triggers several downstream pathways, such as the phosphoinositide 3-kinases (PI3K)-AKT signaling pathway, the phospholipase Cγ1 (PLC-γ1) pathway, and the Ras-mitogen-activated protein kinase (MAPK) pathway. These pathways induce differentiation, maturation, and the survival of neurons[30,31].

The importance of RA in stage I has been widely accepted, while the presence of RA in the stage II remains controversial[14,32–34]. Shipley et al.[33] argued that the presence of RA during maturation is necessary, whereas Dravids et al.[34] suggested RA was unnecessary in stage II of differentiation. Our study indicated the presence of RA during the maturation stage significantly influenced the differentiation and the maturation of SH-SY5Y cells. The FACS analysis (Fig. 2) revealed that the cell would continue proliferating even in maturation stage if RA is absent, leading to an unwanted undifferentiated cell population. Conversely, the presence of RA reduces proliferative capacity and promotes the expression of MAP2, and VGLUT1 aligning with previous reports[35–37].

Alpha-synuclein (a-Syn) plays a pivotal role in synaptic function, specifically in the regulation of neurotransmitter release by binding to synaptic vesicles and modulating their availability. While a-Syn is critical for normal neuronal communication, its dysregulation leads to the formation of Lewy bodies (LBs)—protein aggregates that are pathological hallmarks of neurodegenerative diseases like Parkinson's disease and dementia with Lewy bodies[38]. In our study, we observed a significant increase in *SNCA* mRNA expression, which encodes for a-Syn, particularly in 3D cultures treated with 5% hiFBS and RA. This elevation in SNCA levels correlates with neuronal maturation, as a-Syn is known to play a role in synaptic vesicle cycling and neuronal plasticity, both essential for mature neuronal function. Moreover, our findings suggest that the presence of RA in Stage II influences the upregulation of a-Syn, further supporting its role in neuronal development.

Interestingly, research has shown that varying levels of a-Syn expression can lead to either cell proliferation or cell death, depending on its regulation[39]. This dual nature of a-Syn highlights the importance of controlled expression during neuronal maturation, particularly in the context of NDD research, where a-Syn dysregulation leads to neurotoxicity. In our model, the elevated expression of a-Syn in response to RA treatment suggests a transition toward a mature neuronal phenotype, capable of modeling both normal and pathological conditions seen in NDDs.

While SH-SY5Y cells were established as Parkinson's disease modeling[5,13], our protocol directs the cell into different pathway. By combining effects of B27 and RA, our cells strongly expressed glutamatergic neuron features as presented in FACS analysis (Fig. 2), ICC analysis (Fig. 3A), mRNA expression levels of *GLUL* (Fig. 4). VGLUT1 plays a crucial role in the central nervous system by facilitating the uptake of glutamate into synaptic vesicles, essential for maintaining synaptic efficacy and controlling neuronal activity[23,40]. *GLUL* gene encodes for Glutamate-Ammonia Ligase, which synthesizes glutamine from glutamate and ammonia in an ATP-dependent reaction[7]. Additionally, B27 was found to reduce TH expression[7], which aligns with our FACS results. The cyclic voltammetry results further demonstrated the maturation of glutamatergic neurons by detecting glutamate signals in the spheroids.

The 3D spheroid culture system on PAMCELL™ plates were introduced in our previous report[21]. Each well of the 96-well R100 plate contains over 350 micropads, each with a diameter of 100 μm, allowing for cell migration and the formation of uniformly sized spheroids. These features are suitable not only for large-scale spheroid production but also for high-throughput screening. Additionally, other 3D culture platforms such as hanging drops, bioreactors, and ultra-low attachment plates require careful handling and extensive techniques for downstream applications such as ICC or SEM. These methods often necessitate transferring spheroids to other platforms like cover glass, leading to potential spheroid loss. In contrast, the thin film flat bottom of 3D microarray plate allows users to perform downstream experiments directly on-site, minimizing the risk of cell loss.

Leveraging the advantages of the plate, in this study, we verified the differentiation and maturation process of SH-SY5Y cells in 3D environment and optimized the serum condition specifically for 3D culture. Many reports recommended low serum concentration (2.5–1%) when differentiated SH-SY5Y to avoid cell proliferation[7,13,14,16,33–35]. However, 3D cultures with complex cell-cell interaction and microenvironment require different serum concentration to differentiate and mature the neural spheroid. We found that even after 12-day process, spheroids nurtured with 2.5% hiFBS were only in early stage of differentiation with short and thick neurite extension (Fig. 3). Conversely, 5% hiFBS spheroids provided complex matrix neurite around and inside the spheroid. Additionally, FACS analysis (Fig. 2) mRNA expression levels of 3D 5% hiFBS spheroids also demonstrated that 5% hiFBS is more optimal for the differentiation and maturation of SH-SY5Y spheroids.

To further demonstrate the potential of our system, we utilized a GO enzymatic sensor to measure glutamate neurotransmitter release during both inter-spheroid and intra-spheroid communication. One key feature of neurodegenerative diseases (NDDs) is glutamate excitotoxicity, a process in which excessive extracellular glutamate levels cause synaptic dysfunction and neuronal loss, as seen in the brains of patients with Alzheimer's disease, Huntington's disease and Parkinson's disease[41,42]. Glutamate neurotransmission is regulated in a Ca^{2+}-dependent manner, where the release of glutamate from neurons is triggered by intracellular Ca^{2+} signaling[43].

During cell starvation, there is an increase in intracellular Ca^{2+} concentration, primarily due to the depletion of cellular energy, which impairs calcium homeostasis[44]. The influx of Ca^{2+} leads to excessive glutamate release into the extracellular environment[45]. Additionally, accumulation of Ca^{2+} in the endoplasmic reticulum (ER) and mitochondria during starvation triggers neuronal autophagy, further contributing to the massive release of glutamate[46]. Over time, this excessive glutamate leads to glutamate excitotoxicity. In our system, we measured the increasing glutamate signals via cyclic voltammetry under three conditions: healthy spheroids, 2-day starved spheroids, and 4-day starved spheroids. As starvation-induced Ca^{2+} accumulation intensified, the release of glutamate increased, as indicated by the higher electrochemical signals detected in the starved spheroids.

In conclusion, we developed a refined protocol for differentiating SH-SY5Y cells into glutamatergic neurons using 3D PAMCELL™ microarrays, optimizing serum concentrations and incorporating retinoic acid (RA). Our results highlight RA's crucial role in both differentiation and maturation, significantly enhancing neuronal development and reducing cell proliferation. The expression of glutamatergic markers like VGLUT1 and GLUL confirmed the shift towards a glutamatergic phenotype. The 3D culture system fostered more physiologically relevant cell interactions, essential for proper neuronal development and function, demonstrated by improved glutamate handling. This protocol offers a valuable tool for neurodegenerative disease research and drug development, setting the stage for future studies to refine this approach and explore its broader applications in neurological disorders.

Materials and methods

Cell culture and differentiation

Human neuroblastoma cell lines SH-SY5Y (CRL-2266; 47, XX, +1q) were obtained from American Type Culture Collection (ATCC; Manassas, VA, USA). The cells were proliferated in Eagle's Minimum Essential Medium (EMEM; M4655, Sigma-Aldrich, Burlington, MA, USA) with penicillin and streptomycin and 15% heat-inactivated fetal bovine serum (hiFBS; Thermo Fisher, Waltham, MA, USA). The cells were incubated at 37 °C, 5% CO2, and 95% humidity. When reached 80–90% confluence, cells were passaged with 4 mL of TrypLE™ Express Enzyme (Thermo Fisher) for 5 min, then the enzyme was inhibited via addition of proliferation media. The cells used in experiments were consistently maintained at a passage number below 10.

SH-SY5Y cells were differentiated and matured in 96-well PAMCELL™ R100 plates (ANK, Suwon, Korea) and 12-well culture plates. For neuron spheroid cultures (3D culture), 40,000 cells per well were seeded onto 96-well PAMCELL™ R100 plates, which were pre-coated with iMatrix-511 (1:1000 in PBS) for 1 h. The cells were cultured in EMEM supplemented with various ranges of hiFBS (2.5%, 5%, 10%, 15%), 1× penicillin/streptomycin, and 10 µM retinoic acid (RA; 223018, Sigma-Aldrich). On day 6, the culture medium was replaced with 2 types of maturation media (Neurobasal (21103049, Thermo Fisher), 1% B27 (Thermo Fisher), 20 mM KCl (Sigma-Aldrich), 1% Penicillin, 2mM Glutamax (Thermo Fisher), 0.05 ng/µL Brain-derived neurotrophic factor (BDNF; Sigma-Aldrich): RA-free and RA treated (10 µM) media and half the medium was changed every day until day 12. To obtain conventional two-dimensional monolayer (2D) cultures, cells were cultured on 12-well plates coated with Matrigel Matrix (Corning Inc., NY, USA) at 1: 1000 ratio in ice-cold DMEM/F12 for 1 h. Cells were seeded at 30,000 cells per well, and cultured in EMEM supplemented with 2.5% hiFBS, one penicillin/streptomycin, and 10 µM RA for a period of 6 days, similar to the 3D culture method during the maturation phase. Maturation media was replaced every 48 h during this period (see Scheme 1 for further details).

Immunocytochemistry

After removing the maturation medium, the cells were washed with PBS both before and after the fixation and permeabilization steps, antibodies were then treated as described in protocol[21]. Briefly, the spheroids were fixed with 4% paraformaldehyde (PFA) for one hour and then permeabilized with 0.3% Triton-X 100 for 30 min. Samples were then washed three times in PBS and then soaked in a blocking solution for one hour (50 mM phosphate-buffered saline pH 7.4 (PBS; Thermo Fisher) with 1% bovine serum albumin (BSA; BioWorld, OH, USA). The permeable cells were incubated with primary antibodies against VGLUT, MAP2, TUJ1, EN1, Synapsin for an overnight period at 4 °C (Supplementary Table S1). After washing with blocking buffer, secondary antibodies were treated for 30 min at 4°C. Dihydrochloride 4′,6-Diamidino-2-phenylindole dihydrochloride (DAPI; Thermo Fisher) was incubated for 20 min. The stain must be removed by washing thoroughly three times or more with PBS. To avoid being dried and detached from plates, spheroids are not exposed to air for every single step.

The following above protocol was applied for 2D SHSY5 cells with time adjustment: 15 min for fixation, 10 min for permeability, and 30 min for blocking.

Florescent images were taken using a confocal microscope (Leica Stellaris 5, Leica Camera AG, Germany).

Flow cytometry analysis (FACS)

In 3D PAMCELL™ culture, cells were pipetted to detach from the well and subsequently centrifuged to remove media. Accutase (200 µL for 3D and 1mL for 2D per well; Thermo Fisher) was used to dissociate the spheroids for ten minutes. Observe under a microscope frequently to confirm the separation. Then, the media is added to collect the cell, and the centrifuge is used to remove the media. Followed by 1 h of fixation in 4% PFA. The cells were rinsed three times with PBS, then permeabilized with 0.3% Triton-X 100 for 20 min. After centrifugation to remove the media, the cells were incubated in blocking buffer for one hour and then treated with first antibody for one hour (Supplementary Table S1). Cells were washed 3 times with blocking buffer, followed by a second antibody and incubated for 30 min. FACS solution (50 mM PBS containing 1% BSA, 10% fetal bovine serum (FBS) for 30 min at 4 °C after washing.

RNA extraction, cDNA conversion and qRT-PCR

The mRNA content of differentiated SHSY5 cells was extracted on day 12 using the following method[21]. After removing media from the cells, total RNA was extracted using the Total RNA Extraction Kit (iNtRON Biotechnology, Inc., South Korea), then quantified with NanoDrop One (Thermo Fisher). RNA was converted to cDNA using RT-PCR machine was performed following the manufacturer's instructions using Maxime™ RT PreMix (Random Primer) (iNtRON Biotechnology, Inc.). In all qRT-PCR reactions, the AriaM x Real-Time PCR system was used with 1 µL of cDNA template, 7 µL of ultra-distilled water, 10 µL of RealMOD green W2 qPCR mix (iNtRON Biotechnology, Inc.), and 1 µL of forward and reverse primers. Supplementary information regarding primers can be found in the following section. Information of primers were used was described in the Supplementary Table S2. The PCR settings included an initial denaturation at 95 °C for 10 min, followed by 40 cycles of denaturation at 95 °C for 20 s, annealing at 55 °C for 40 s, and a melt curve analysis with one cycle each at 95 °C for 10 s, 65 °C for 10 s, and 95 °C for 10 s. The qPCR results were visualized using Agilent Aria 1.8, and relative expression levels were normalized to GAPDH. Ct values obtained through RT-PCR can be found in Supplementary Table S4.

Neurite length analysis

MAP2 immunochemistry images were taken for neurite length analysis. 2 spheroids were analyzed in each type of samples (5% hiFBS and 2.5% hiFBS). Neurite tracing analysis were performed using *FIJI* software with AutoNeuriteJ plugin[47]. Prior to analysis, a scale of 700 pixels to 100 µm was applied to each image using the *FIJI* software.

Glutamate oxidase (GO) electrodes preparation for glutamate level detection

Glutamate oxidase (GO) solution was prepared before enzyme immobilization. First, 1 mL of sodium periodate (1.5 mg/mL in PBS; Sigma-Aldrich) was added to a vial of GO (25 units/vial; Yamasa Corp., Japan). The solution was then stirred at 4 °C for 1 h. Excess chemicals were washed away with PBS. The periodate-oxidized enzyme was collected using a 30 kDa MWCO Amicon® Ultra Centrifugal Filter (Millipore Corp., USA) and resuspended in 50 mM PBS pH 7.4. The solution was stored at 4 °C.

A platinum electrode was polished with alumina slurry (0.05 µm, BASi Corp., USA) and incubated with 20 mM cystamine solution (Sigma-Aldrich) for 12 h at room temperature after being washed with double-distilled water (DDW). The cystamine-functionalized electrode was then treated in GO solution for 1 h at room temperature, resulting in immobilization through Schiff-base formation. The GO-immobilized electrode was washed and stored in PBS prior to use.

The maturation media was exchanged 6 h before testing. Electrochemical characterization was conducted using cyclic voltammetry. With the selected anodic oxidation potential of E_{app} (0.65 V vs. Ag/AgCl reference electrode), glutamate concentration in the testing sample was evaluated.

Statistical analysis

All statistical analyses were performed using GraphPad Prism version 9.0.0 (GraphPad, CA, USA). The size of the spheroids was measured by Fiji. Data are shown as the mean ± standard error of the mean. Student's t-test and one-way analysis of variance (ANOVA) were applied and a p-value of $p \leq 0.05$, 0.01, and 0.001 was considered significant.

Data availability

The data sets used and/or analyzed during the current study are available from the corresponding author upon reasonable request. Results of the size of spheroids can be found in the Supplementary Table 3. mRNA expression level can be found in the Supplementary Table 4. Voltammogram raw data can be found in the Supplementary Table 5. MAP2 neurite length data can be found in Supplementary Table 6.

Received: 18 August 2024; Accepted: 18 November 2024
Published online: 25 November 2024

References

1. *Global Status Report on the Public Health Response to Dementia Methodology for Producing Global Dementia Cost Estimates*. (2021). http://apps.who.int/bookorders
2. Dawson, T. M., Golde, T. E. & Lagier-Tourenne, C. Animal models of neurodegenerative diseases. *Nat. Neurosci.* **2018 2110 21**, 1370–1379 (2018).
3. Ghaedi, M. & Niklason, L. E. Human pluripotent stem cells (iPSC) generation, culture, and differentiation to lung progenitor cells. *Methods Mol. Biol.* **1576**, 55 (2019).
4. Hansford, L. M. et al. Neuroblastoma cells isolated from bone marrow metastases contain a naturally enriched tumor-initiating cell. *Cancer Res.* **67**, 11234–11243 (2007).
5. Xicoy, H., Wieringa, B. & Martens, G. J. M. The SH-SY5Y cell line in Parkinson's disease research: a systematic review. *Mol. Neurodegener.* **12**, 1–11 (2017).
6. Kovalevich, J. & Langford, D. Considerations for the Use of SH-SY5Y Neuroblastoma cells in Neurobiology. *Methods Mol. Biol.* **1078**, 9–21 (2013).
7. Martin, E. R., Gandawijaya, J. & Oguro-Ando, A. A novel method for generating glutamatergic SH-SY5Y neuron-like cells utilizing B-27 supplement. *Front. Pharmacol.* **13**, 943627 (2022).
8. Lopes, F. M. et al. Comparison between proliferative and neuron-like SH-SY5Y cells as an in vitro model for Parkinson disease studies. *Brain Res.* **1337**, 85–94 (2010).
9. Filograna, R. et al. Analysis of the Catecholaminergic phenotype in Human SH-SY5Y and BE(2)-M17 neuroblastoma cell lines upon differentiation. *PLoS One.* **10**, e0136769 (2015).

10. Venkataraman, L., Fair, S. R., Mcelroy, C. A., Hester, M. E. & Fu, H. Modeling neurodegenerative diseases with cerebral organoids and other three-dimensional culture systems: focus on Alzheimer's disease. doi: (2015). https://doi.org/10.1007/s12015-020-10068-9/Published
11. Teppola, H., Sarkanen, J. R., Jalonen, T. O. & Linne, M. L. Morphological differentiation towards neuronal phenotype of SH-SY5Y Neuroblastoma cells by Estradiol, retinoic acid and cholesterol. *Neurochem Res.* **41**, 731–747 (2016).
12. Mazzoccoli, C. et al. N-acetylaspartate (NAA) induces neuronal differentiation of SH-SY5Y neuroblastoma cell line and sensitizes it to chemotherapeutic agents. *Oncotarget* **7**, 26235 (2016).
13. Ioghen, O. C., Ceafalan, L. C. & Popescu, B. O. SH-SY5Y Cell Line in Vitro models for Parkinson Disease Research-Old Practice for New trends. *J. Integr. Neurosci.* **22**, (2023).
14. Kaya, Z. B. et al. Optimizing SH-SY5Y cell culture: exploring the beneficial effects of an alternative media supplement on cell proliferation and viability. *Sci. Rep. 2024*. **141 14**, 1–11 (2024).
15. Strother, L., Miles, G. B., Holiday, A. R., Cheng, Y. & Doherty, G. H. Long-term culture of SH-SY5Y neuroblastoma cells in the absence of neurotrophins: a novel model of neuronal ageing. *J. Neurosci. Methods*. **362**, 109301 (2021).
16. Lopez-Suarez, L., Awabdh, S., Al, Coumoul, X. & Chauvet, C. The SH-SY5Y human neuroblastoma cell line, a relevant in vitro cell model for investigating neurotoxicology in human: focus on organic pollutants. *Neurotoxicology* **92**, 131–155 (2022).
17. Palanivel, V. et al. Neuroprotective effects of Neuropeptide Y on Human Neuroblastoma SH-SY5Y cells in glutamate excitotoxicity and ER stress conditions. *Cells* **11**, 3665 (2022).
18. de Medeiros, L. M. et al. Cholinergic differentiation of Human Neuroblastoma SH-SY5Y Cell Line and its potential use as an in vitro model for Alzheimer's Disease studies. *Mol. Neurobiol.* **56**, 7355–7367 (2019).
19. Agholme, L., Lindström, T., Kgedal, K., Marcusson, J. & Hallbeck, M. An in vitro model for neuroscience: differentiation of SH-SY5Y cells into cells with morphological and biochemical characteristics of mature neurons. *J. Alzheimers Dis.* **20**, 1069–1082 (2010).
20. Falkenburger, B. H. & Schulz, J. B. Limitations of cellular models in Parkinson's disease research. *J. Neural Transm Suppl.* 261–268. https://doi.org/10.1007/978-3-211-45295-0_40 (2006).
21. Pham, H. T. M. et al. A novel and cost-effective method for high-throughput 3D culturing and rhythmic assessment of hiPSC-derived cardiomyocytes using retroreflective Janus microparticles. *Biomater. Res.* **27**, 1–18 (2023).
22. Lee, S. et al. Enhancement of anti-inflammatory and immunomodulatory effects of adipose-derived human mesenchymal stem cells by making uniform spheroid on the new nano-patterned plates. *Biochem. Biophys. Res. Commun.* **552**, 164–169 (2021).
23. Martineau, M., Guzman, R. E., Fahlke, C. & Klingauf, J. VGLUT1 functions as a glutamate/proton exchanger with chloride channel activity in hippocampal glutamatergic synapses. *Nat. Commun.* **2017 81 8**, 1–13 (2017).
24. Yamaguchi, T., Sheen, W. & Morales, M. Glutamatergic neurons are present in the rat ventral tegmental area. *Eur. J. Neurosci.* **25**, 106–118 (2007).
25. Du, X. et al. Research progress on the role of type i vesicular glutamate transporter (VGLUT1) in nervous system diseases. *Cell. Biosci.* **10**, 1–10 (2020).
26. Harada, A., Teng, J., Takei, Y., Oguchi, K. & Hirokawa, N. MAP2 is required for dendrite elongation, PKA anchoring in dendrites, and proper PKA signal transduction. *J. Cell. Biol.* **158**, 541 (2002).
27. Thiel, G., Synapsin, I. & Synapsin, I. I. Marker proteins of synaptic vesicles. *Brain Pathol.* **3**, 87–95 (1993).
28. Allodi, I., Montañana-Rosell, R., Selvan, R., Löw, P. & Kiehn, O. Locomotor deficits in a mouse model of ALS are paralleled by loss of V1-interneuron connections onto fast motor neurons. *Nat. Commun.* **12**, 1–18 (2021).
29. Nakamura, T., Gu, Z. & Lipton, S. A. Contribution of glutamatergic signaling to nitrosative stress-induced protein misfolding in normal brain aging and neurodegenerative diseases. *Aging Cell.* **6**, 351–359 (2007).
30. Jin, W. Regulation of BDNF-TrkB signaling and potential therapeutic strategies for Parkinson's Disease. *J. Clin. Med.* **9**, (2020).
31. Huang, E. J. & Reichardt, L. F. Trk receptors: roles in neuronal signal transduction. *Annu. Rev. Biochem.* **72**, 609–642 (2003).
32. Encinas, M. et al. Sequential treatment of SH-SY5Y cells with retinoic acid and brain-derived neurotrophic factor gives rise to fully differentiated, neurotrophic Factor-Dependent, human neuron-like cells. *J. Neurochem.* **75**, 991–1003 (2000).
33. Shipley, M. M., Mangold, C. A. & Szpara, M. L. Differentiation of the SH-SY5Y human neuroblastoma cell line. *J. Vis. Exp.* e53193 (2016). (2016).
34. Dravid, A., Raos, B., Svirskis, D. & O'Carroll, S. J. Optimised techniques for high-throughput screening of differentiated SH-SY5Y cells and application for neurite outgrowth assays. *Sci. Rep. 2021*. **111** (11), 1–15 (2021).
35. Kunzler, A. et al. Changes in cell cycle and Up-Regulation of neuronal markers during SH-SY5Y Neurodifferentiation by Retinoic Acid are mediated by reactive species production and oxidative stress. *Mol. Neurobiol.* **54**, 6903–6916 (2017).
36. Horvat, L. et al. *Hv L Mol. Exp. Biol. Med.* **1**, 38–43 (2019).
37. Waetzig, V. et al. Retinoic acid–induced survival effects in SH-SY5Y neuroblastoma cells. *J. Cell. Biochem.* **120**, 5974–5986 (2019).
38. Wang, J., Wang, F., Mai, D. & Qu, S. Molecular mechanisms of Glutamate Toxicity in Parkinson's Disease. *Front. Neurosci.* **14**, (2020).
39. Rodríguez-Losada, N. et al. Overexpression of alpha-synuclein promotes both cell proliferation and cell toxicity in human SH-SY5Y neuroblastoma cells. *J. Adv. Res.* **23**, 37–45 (2020).
40. Benarroch, E. E. Glutamate transporters: diversity, function, and involvement in neurologic disease. *Neurology* **74**, 259–264 (2010).
41. Danysz, W. & Parsons, C. G. Alzheimer's disease, β-amyloid, glutamate, NMDA receptors and memantine–searching for the connections. *Br. J. Pharmacol.* **167**, 324–352 (2012).
42. Lewerenz, J. & Maher, P. Chronic glutamate toxicity in neurodegenerative diseases-what is the evidence? *Front. Neurosci.* **9**, (2015).
43. Popoli, M., Gennarelli, M. & Racagni, G. Modulation of synaptic plasticity by stress and antidepressants. *Bipolar Disord.* **4**, 166–182 (2002).
44. Machaca, K. Ca 2 + signaling, genes and the cell cycle. doi: (2010). https://doi.org/10.1016/j.ceca.2010.10.003
45. Maher, P. et al. The role of Ca2 + in cell death caused by oxidative glutamate toxicity and ferroptosis. *Cell. Calcium*. **70**, 47 (2018).
46. Loncke, J. et al. Balancing ER-mitochondrial Ca2 + fluxes in health and disease. *Trends Cell. Biol.* **31**, 598 (2021).
47. Boulan, B. et al. AutoNeuriteJ: an ImageJ plugin for measurement and classification of neuritic extensions. *PLoS One*. **15**, e0234529 (2020).

Author contributions

HTMP, DLN, and MPTL conceived and designed the project. HTMP, DLN, MPTL, and KWL performed research, conducted data analyses, and created figures. HTMP, DLN wrote the manuscript. JHK and HCY discussed the results, consulted, and gave critical feedback. All the authors read and approved the manuscript.

Funding

This study was supported by the Creative Materials Discovery Program (NRF-2019M3D1A1078943), the Priority Research Centers (NRF-2019R1A6A1A11051471), and the Commercialization Promotion Agency for R&D Outcomes (COMPA) grant funded by the Korean government (MSIT) (no. 2021N100), and the Materials-components Technology Development Project (KEIT-20026474) funded by the Korean Government (MOTIE).

Declarations

Competing interests
The authors declare no competing interests.

Additional information
Supplementary Information The online version contains supplementary material available at https://doi.org/10.1038/s41598-024-80369-3.

Correspondence and requests for materials should be addressed to H.C.Y. or H.T.M.P.

Reprints and permissions information is available at www.nature.com/reprints.

Publisher's note Springer Nature remains neutral with regard to jurisdictional claims in published maps and institutional affiliations.